Photoassociation and coherent transient dynamics in the interaction of ultracold rubidium atoms with shaped femtosecond pulses. II. Theory

Andrea Merli, Frauke Eimer, Fabian Weise, and Albrecht Lindinger
Institut für Experimentalphysik, Freie Universität Berlin, Arnimallee 14, D-14195 Berlin, Germany

Wenzel Salzmann, Terry Mullins, Simone Götz, Roland Wester, and Matthias Weidemüller[*]
Physikalisches Institut, Universität Freiburg, Hermann Herder Str. 3, D-79104 Freiburg, Germany

Ruzin Ağanoğlu and Christiane P. Koch[†]
Institut für Theoretische Physik, Freie Universität Berlin, Arnimallee 14, D-14195 Berlin, Germany

Photoassociation of ultracold rubidium atoms with femtosecond laser pulses is studied theoretically. The spectrum of the pulses is cut off in order to suppress pulse amplitude at and close to the atomic resonance frequency. This leads to long tails of the laser pulse as a function of time giving rise to coherent transients in the photoassociation dynamics. They are studied as a function of cut-off position and chirp of the pulse. Molecule formation in the electronically excited state is attributed to off-resonant excitation in the strong-field regime.

PACS number(s): 32.80.Qk, 34.50.Rk

I. INTRODUCTION

Cooling, trapping, and manipulation of atoms and molecules in the ultracold regime ($T \leq 100$ μK) represents one of the most active research fields in contemporary atomic, molecular, and optical physics. Photoassociation is the formation of molecules when two colliding atoms are excited by laser light into bound vibrational levels of an electronically excited state. Using continuous-wave lasers, photoassociation of ultracold atoms can be employed to study collisional properties of ultracold atoms, in particular long-range potential-energy curves [1]. If followed by spontaneous emission, it also serves to form ultracold molecules in their electronic ground state [2].

The use of short laser pulses for photoassociation of ultracold atoms has been suggested in theory work for about a decade [3–10]. Initially, the main goal was to find a photoassociation scheme that would allow for larger formation rates of excited-state molecules [4,5]. In order to coherently produce ultracold molecules in their electronic ground state, the pump-dump scenario was adapted to photoassociation [6–8]: A pump pulse creates a vibrational wave packet on the electronically excited state which travels toward its inner turning point where it is sent to the ground state by the dump pulse. Other coherent control schemes such as adiabatic passage [9] and pulse optimization using genetic algorithms were investigated as well [10]. Coherent photoassociation using short laser pulses is closely linked to the ultimate goal of ultracold molecule formation, the stabilization of the molecules into their vibrational ground state [11–14]. This has

been discussed in theory work in the context of optimal control [15] and coherent pulse accumulation [16].

In the theoretical studies on short-pulse photoassociation, pulses with a spectral bandwidth of a few wave numbers were suggested. This choice is motivated by the requirement of exciting a narrow band of transitions with large free-bound Franck-Condon factors close to the atomic resonance without exciting atomic transitions. This spectral bandwidth corresponds to transform-limited pulse durations of a few picoseconds. However, pulse shaping capabilities for such pulses have yet to be developed.

Femtosecond pulses on the other hand can be shaped with a number of techniques, but they have a very broad spectrum, addressing both molecular and atomic transitions. However, the probability of atomic transitions is several orders of magnitude larger than that of photoassociation transitions connected to these atomic transitions. Therefore the spectral amplitude of the pulse at the atomic resonance frequency needs to be completely suppressed. Otherwise the atoms would be excited and no molecular signal could be recorded. This suppression of atomic transitions is most easily achieved by putting a knife edge into the Fourier plane of the pulse shaper [17]. The corresponding sharp cutoff in the spectrum of the femtosecond pulse leads to long tails of the pulse as a function of time and induces coherent transient dynamics [18,19]. The transients are reflected in oscillations of the molecular population and can be measured by ionization detection of the excited-state molecules [20]. Photoassociation of ultracold atoms with shaped femtosecond laser pulses has thus been demonstrated recently in a breakthrough experiment [20].

This paper presents a detailed explanation of the experimental results obtained by femtosecond photoassociation of ultracold rubidium atoms with shaped pulses based on theoretical calculations. The details of the experimental setup as well as the major part of the experimental results are found in Ref. [21]. Figure 1 depicts the proposed photoassociation

---

[*]Present address: Physikalisches Institut, Ruprecht-Karls-Universität Heidelberg, Philosophenweg 12, D-69120 Heidelberg, Germany.
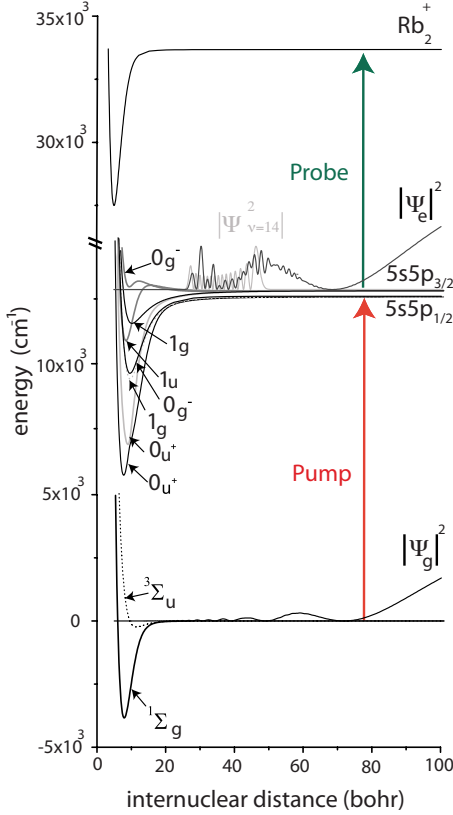
[†]Corresponding author; ckoch@physik.fu-berlin.de

FIG. 1. (Color online) Scheme of the femtosecond pump-probe sequence involving the Rb_2 potential-energy curves of the electronic ground state, the attractive potentials of the first electronically excited state correlating to the $5s+5p_{1/2}$ and $5s+5p_{3/2}$ asymptotes, and the cationic state of Rb_2^+. The initial scattering state, the wave function amplitude after the pump pulse and one sample excited-state vibrational wave function $[v'=14$ of the $0_g^-(5s+5p_{3/2})$ state] are also depicted.

mechanism including the potential-energy curves considered in the calculations. A first laser field (the pump pulse indicated by the red arrow) excites two atoms from their ground state $(5s+5s)$ into long-range bound molecular levels of an electronically excited state (correlated with the $5s+5p_{1/2}$ or $5s+5p_{3/2}$ asymptotes). The initial scattering state with a relative scattering energy corresponding to the trap temperature of 100 μK is shown on the ground state. The excited-state wave function after the pulse is over (at $t=t_{max}+17.5$ ps [22]) as well as one exemplary excited-state vibrational wave function is displayed in the first excited state of Fig. 1. In order to detect the excited-state molecules, a second laser field (the probe pulse indicated by the green arrow) transfers them to the ionic state.

The paper is organized as follows: Sec. II briefly reviews the theoretical description of two rubidium atoms excited by a photoassociation laser pulse. The photoassociation mechanism based on strong-field off-resonant excitation is described in detail in Sec. III while the coherent transient dynamics are studied in Sec. IV. Theoretical and experimental results are compared in Secs. V and VI concludes.

II. THEORETICAL APPROACH

In order to gain detailed insight into the mechanism of femtosecond photoassociation, the pump excitation step was simulated in quantum dynamical calculations of the light-molecule interaction. The pump pulse transfers population between the ground and first excited electronic states. The probe step was not explicitly taken into account. Rather, it was assumed that any population of the first excited state is ionized alike.

In a two-channel picture, the Hamiltonian describing two rubidium atoms subject to excitation by a laser field in the dipole and rotating-wave approximations is given by

$$\hat{H} = \begin{pmatrix} \hat{T} + V_g(\hat{R}) & \hat{\mu}E(t) \\ -\hat{\mu}E(t)^* & \hat{T} + V_e(\hat{R}) - \Delta \end{pmatrix}. \quad (1)$$

Here, $\hat{R}$ denotes the internuclear distance, $\hat{T}$ denotes the kinetic-energy operator, and $V_{g/e}$ denotes the ground- and excited-state potential-energy curves. The parameter $\Delta = \hbar(\omega_0 - \omega_L)$ represents the detuning of the pump pulse central frequency relative to the $5s+5p_{1/2}$ and $5s+5p_{3/2}$ asymptotes, respectively. The off-diagonal elements of the Hamiltonian describe the electric dipole coupling with $\hat{\mu}$ denoting the transition dipole and $E(t)$ denoting the electric field of the pump pulse. The R dependence of the transition dipole was neglected which is justified for excitation at long range.

A two-channel picture assumes that no couplings between electronic states, for example, due to spin-orbit interaction, play a role on the time scale of the dynamics. It is then possible to consider pairwise combinations of ground and excited electronic states in Eq. (1). An analysis of the dynamics has confirmed that this assumption is justified: the dynamics are purely long range and dominated by electronic transitions due to the laser field.

The potential-energy curves are taken from Ref. [23] and matched to the long-range dispersion potentials, $(C_3/R^3+)C_6/R^6+C_8/R^8+C_{10}/R^{10}$ with the C_n coefficients found in Refs. [24,25]. Potential-energy curves in the Hund's case (c) representation were obtained by approximating the spin-orbit couplings by their asymptotic values and subsequent diagonalization, see, e.g., Ref. [26]. Of all potential curves correlating to the $5s+5p_{1/2}$ and $5s+5p_{3/2}$ asymptotes, those with attractive character and dipole-allowed transitions were taken into account (0_g^-, 1_g, 0_u^+, and 1_u correlating to the $5s+5p_{1/2}$ asymptote and 0_g^-, 1_g, 0_u^+, and 1_u correlating to the $5s+5p_{3/2}$ asymptote). Moreover simulations were also performed for two repulsive potential-energy curves, those of the $1_u(5s+5p_{3/2})$ and $2_g(5s+5p_{3/2})$ states. Note that the excited-state potentials differ by their effective C_3 coefficients and strengths of transition dipole moment.

Hamiltonian (1) is represented on a mapped Fourier grid [27,28]. Vibrational wave functions are obtained by diagonalizing the Hamiltonian with $E(t)$ set to zero. As an example, a vibrational wave function localized in the long-range well of the $0_g^-(5s+5p_{3/2})$ excited state, with $v=14$, is shown in Fig. 1. The photoassociation dynamics were studied by numerically solving the time-dependent Schrödinger equation (TDSE),
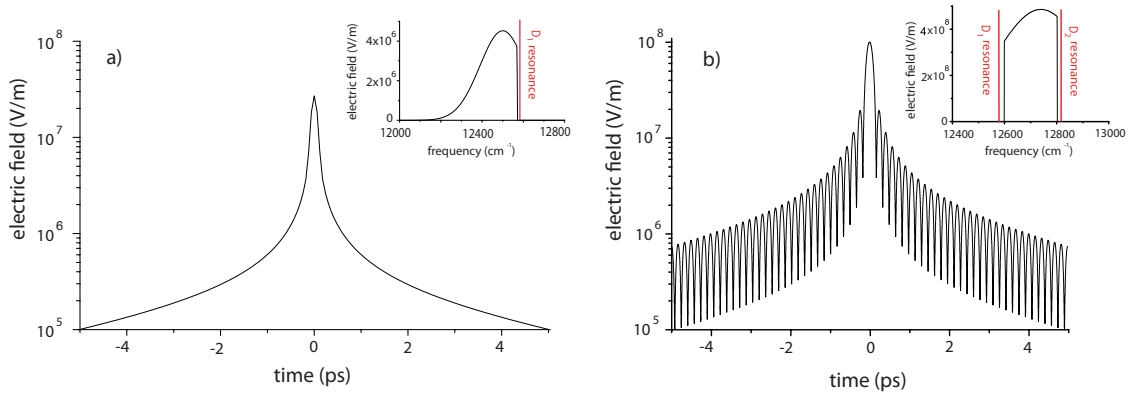
FIG. 2. (Color online) Temporal field envelope of cut pump pulse spectrum (shown in the insets) below the (a) D_1 and (b) D_2 atomic resonance. Tails to both sides of the peak are caused by the spectral cutoff.

$$i\hbar\frac{\partial}{\partial t}\begin{pmatrix}\Psi_g(R;t)\\\Psi_e(R;t)\end{pmatrix}=\hat{\mathbf{H}}\begin{pmatrix}\Psi_g(R;t)\\\Psi_e(R;t)\end{pmatrix},\qquad(2)$$

using the Chebyshev propagator [29]. $\Psi_{g/e}(R;t)$ denotes the ground- (excited-) state component of the time-dependent wave function. The initial state is taken to be the scattering state with scattering energy closest to $E_{scatt}/k_B=T_{trap}$, where k_B denotes the Boltzmann constant and T_{trap} denotes the temperature of the trap. In principle an average over all thermally populated scattering states needs to be performed [8]. However, it will turn out in our simulations that the dynamics are dominated by electronic transitions and the different nodal structures of the scattering states at very large distances do not play a role. Simulations for a single initial state are therefore sufficient.

The pulses entering Eqs. (1) and (2) were obtained similar to the experimental procedure. In the experiment an optical low-pass filter was employed in the Fourier plane of the zero dispersion compressor to manipulate the spectral shape of the pump pulse close to the D_1 or D_2 atomic line in such a way that all frequencies above the chosen atomic resonance, the respective resonance frequency itself, and some frequencies below this particular line were cut off. This is done in order to prevent the loss of the captured atoms due to resonant three-photon ionization and photon pressure [17]. In the case of excitation near the D_2 line, perturbing frequencies near the D_1 atomic resonance arising from the large spectral bandwidth of the femtosecond pulse were also removed from the pump pulse spectrum. In order to model those experimental pump pulses, a Gaussian transform-limited laser field is subjected to one or two cuts of spectral amplitude in the frequency domain. The sharp cuts lead to very long transients of the pulse in the time-domain representation, cf. Fig. 2, i.e., the temporal behavior strongly deviates from the original time profile. The pulse has long tails, reaching out to a few picoseconds before and after the maximum as shown in Fig. 2. Within the tails, the electric field oscillates with a frequency that matches the spectral cut-off frequency, cf. Fig. 4. If two cuts are applied, the tails show a beat pattern that depends on the specific cut positions, cf. Fig. 2(b). The influence of the specific shape of the pump pulses in time and frequency domain on the dynamics will be discussed in Sec.

IV. The parameters defining the pulse are the central wavelength, spectral width, energy, linear chirp rate, and spectral cut-off positions.

The time-dependent population of the first electronically excited state is calculated as weighted sum of the possible transitions from the singlet ground and lowest triplet state with the ratio 1:3. In order to take the finite duration of the probe pulse into account, the measured ion signal was obtained by convoluting the time-dependent excited-state population with a Gaussian of 500 fs full width at half maximum (FWHM) [30].

III. PHOTOASSOCIATION

The photoassociation dynamics is illustrated in Fig. 1 by the nuclear wave functions, $\Psi_g(R;t)$ and $\Psi_e(R;t)$, in the ground- and excited-state potentials when the pulse is over at about $t=17.5$ ps after the pump pulse maximum. The $a\Sigma_u^+(5s+5s)$ lowest triplet state and $0_g^-(5s+5p_{3/2})$ excited state were employed in this example. Pump pulse parameters such as pulse energy and cut-off position correspond to those used in the actual experiment. Specifically, the cut-off positions for the example displayed in Figs. 1 and 3(b) were −15 and −218.3 cm^{-1} below the D_2 resonance, the central wavelength $\lambda_L=785$ nm, spectral bandwidth $\Delta\lambda_L=25$ nm, laser power $P=30$ mW, repetition rate 100 kHz and beam radius $r_B=300$ μm, corresponding to a peak field amplitude of 99 MV/m. Inspection of Fig. 1 reveals that no nuclear dynamics has taken place on the time scale of the pulse including its long tails: the excited-state wave packet, created by the pump pulse, completely reflects the nodal structure of the initial scattering state at long range. This is not surprising since the vibrational periods of weakly bound excited-state levels are on the order of several tens of picoseconds, while the ground-state dynamics evolves even more slowly.

The excited-state wave packet at a certain time can be projected onto the vibrational eigenfunctions of the corresponding excited-state potential. This yields the vibrational distribution and proves that photoassociation, i.e., the excitation of free-colliding atoms into bound levels of an excited state, has taken place. The vibrational distribution after the pulse is shown for the $0_u^+(5s+5p_{1/2})$ state in Fig. 3(a) and for
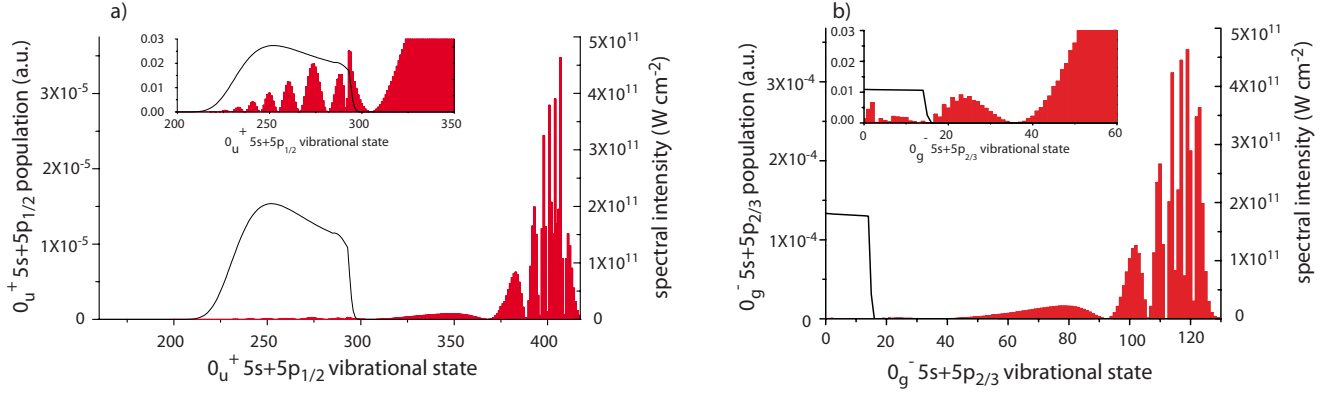
FIG. 3. (Color online) Calculated population distribution in the excited (a) $0_u^+(5s+5p_{1/2})$ and (b) $0_g^-(5s+5p_{3/2})$ states (shaded curves). The solid line displays the spectral pump pulse amplitude where the transition energies from the initial ground-state scattering state to the bound excited-state vibrational levels were matched to the pump pulse spectrum.

the $0_g^-(5s+5p_{3/2})$ state in Fig. 3(b). The cut-off position was chosen to be 15 cm^{-1} below the respective atomic resonance, i.e., below the D_1 line frequency in Fig. 3(a) and below the D_2 line frequency in Fig. 3(b). In Fig. 3(a), the vibrational distribution is characterized by a maximum near $v'=400$. These vibrational levels have large bond lengths on the order of $1000a_0$ and low binding energies of about 1 GHz or 0.03 cm^{-1}. They lie energetically above the spectral cut-off of the pulse. Their population therefore necessarily arises from off-resonant excitation. This is caused by the high peak intensity of the pump pulse. Only a small fraction of the total excited-state population resides in vibrational levels that are resonant within the pump pulse spectrum. For a spectral cut-off detuned by -15 cm^{-1} from the atomic line, resonant excitation occurs for vibrational levels below $v'=290$, cf. inset of Fig. 3(a). Compared to the weakly bound, long-range levels around $v'=400$, their population is suppressed by two orders of magnitude. This is due to much smaller free-bound Franck-Condon factors. The distribution among these levels reproduces the weak-field result, i.e., it is proportional to the Franck-Condon factors multiplied by the spectral envelope of the pump pulse [10,31]. The apparent contradiction of producing within one calculation weak-field (below $v'=290$) and strong-field (near $v'=400$) results is easily resolved by noting that the decisive quantity is the Rabi frequency, i.e., the product of transition dipole and electric field. Since the Franck-Condon factors vary over several orders of magnitude, qualitatively different results are obtained for different regions of the excited-state vibrational spectrum.

A pattern similar to that of the D_1 line results is observed for the D_2 line, cf. Figs. 3(a) and 3(b). In this case, the excited-state potential, the purely long-range $0_g^-(5s+5p_{3/2})$ state, is only about 28 cm^{-1} deep and resonant excitation occurs for vibrational levels below $v'=15$. Due to the shallowness of the potential, only a small part of the pulse spectrum serves for excitation, cf. the inset of Fig. 2(b). If an excited-state potential with a deep minimum such as that of the 1_g [$5s+5p_{3/2}$ state is employed (data not shown), a picture equivalent to Fig. 3(a) emerges]. In both cases the vibrational spectrum is dominated by levels which are off-resonantly excited, above $v'=90$ for the $0_g^-(5s+5p_{3/2})$ state

(with binding energies of less than 0.05 cm^{-1} or 1.5 GHz). It is instructive to compare the amplitudes of the excited-state vibrational level with $v'=14$ and the excited-state wave packet after the pulse, shown in Fig. 1, to the vibrational distributions of Fig. 3(b). The short-range part of the wave packet at internuclear distances $R \lesssim 50a_0$ corresponds to vibrational levels with $v' \leq 14$. The total excited-state population is dominated by the weakly bound levels and electronically excited continuum states. Population of the latter, however, corresponds to excitation of the initial colliding atom pair to an excited pair of free atoms and cannot be regarded as photoassociation.

IV. COHERENT TRANSIENT DYNAMICS

Solving the time-dependent Schrödinger equation allows for a detailed study and analysis of the dynamics induced by the pump pulse. Figure 4 displays the excited-state population, $\int dR |\Psi_e(R;t)|^2$, and the frequency of the induced dipole, i.e., the derivative of the time-dependent phase, $\phi_{\langle\mu\rangle(t)}$, of $\int dR \Psi_g^*(R;t)\hat{\boldsymbol{\mu}}\Psi_e(R;t)\rangle$ [red dashed lines in Figs. 4(a), 4(c), 4(d), and 4(f)] as a function of time and compares them to the envelope and the instantaneous frequency of the pump pulse [black solid lines in Figs. 4(a), 4(c), 4(d), and 4(f)]. Also shown is the relative phase between the transition dipole and the field, i.e., $\phi_{\langle\mu\rangle(t)} - \phi_{E(t)}$ [solid black line in Fig. 4(b)]. Characteristic oscillations of the excited-state population are observed which are due to the long tails of the electric field with cut spectrum, cf. Fig. 4(c). They correspond to the coherent transients [31] that have been observed before in the excitation of atoms with short pulses, see, e.g., Refs. [18,19]. Note that in our case, a molecular signal is observed in the ionization detection [21].

The transient interaction of the weakly bound molecule and the pulse is governed by the induced transition dipole, in particular by the relative phase between the induced dipole and the field. The dynamics obtained for a single spectral cut, i.e., for excitation below the D_1 line (left-hand side of Fig. 4), is discussed first. In this case, the instantaneous frequency of the laser pulse, shown by the black solid line in Fig. 4(a), coincides with the cut-off frequency before and after the pulse maximum but dips to 12 250 cm^{-1} during the main
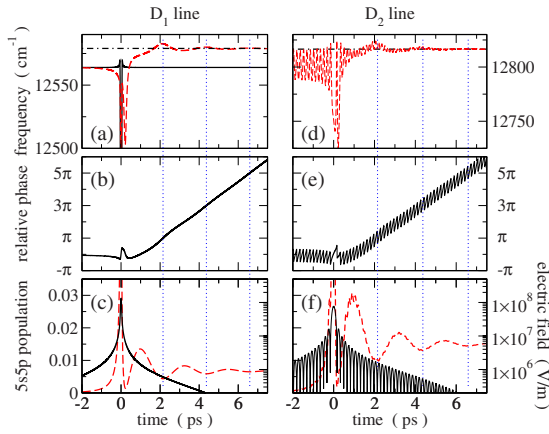
FIG. 4. (Color online) Details of ultrafast dipole dynamics. $a+d$: instantaneous frequency of the pump pulse (solid black line), frequency of induced dipole (dashed red line), position of the D_1, respectively, D_2, resonance frequency (dash-dotted line). $b+e$: relative phase between dipole and light field. $c+f$: electric field envelope of pump pulse (solid black line), excited-state population (dashed red line) for the (c) $0_u^+(5s+5p_{1/2})$ state and (f) $0_g^-(5s+5p_{3/2})$. The vertical dotted blue lines indicate the position where the relative phase crosses $(n+1)\pi$, $n=0,1,2$.

part of the pulse. The depth of the dip is determined by the spectral bandwidth of the pulse. The temporal tails to both sides of the main pulse peak lead to significant field amplitude that oscillates with the cutoff frequency, cf. black solid line in Fig. 4(a). During the main peak of the pulse, around $t=0$, a dipole is induced by off-resonant excitation. It is at first driven by the strong electric field and follows its oscillation. After the main peak of the pulse is over, the coupling is reduced and the dipole oscillates with its intrinsic frequency close to the D_1 resonance frequency, cf. red dashed line in Fig. 4(a). This is due to the excited-state population being dominantly in vibrational levels close to the dissociation limit, cf. Sec. III. The oscillation of the excited-state population goes through one period as the relative phase between dipole and field changes by 2π, see the dotted blue lines and the red dashed curve in Fig. 4(c). The dotted blue lines indicate the times when the relative phase crosses odd integer multiples of π. These times coincide with the minima in the oscillation of the excited-state population. In the long pulse tail, this oscillation results from a beating between the transition dipole and the field that is oscillating with the cutoff frequency. As the long tail of the pump pulse decays [black solid line in Fig. 4(c)], the oscillations of the transition dipole subside as well. This damps effectively the oscillations in the excited-state population since the energy exchange between pulse and molecule vanishes.

The dynamics observed for a pulse to which two spectral cuts are applied, i.e., for excitation below the D_2 resonance frequency (right-hand side of Fig. 4 with $\omega_{c1}=-218$ cm^{-1} and $\omega_{c2}=-15$ cm^{-1} relative to the $5s+5p_{3/2}$ asymptote), is overall similar to that obtained for excitation below the D_1 resonance frequency. However, two spectral cuts lead to a distinct beat pattern in the amplitude and phase of the electric field which carries over to the dynamical observables, namely, transition dipole and excited-state population. The

beat pattern is determined by the positions of the two cuts relative to the carrier frequency of the field. The induced dipole oscillates around the cut position before the main peak of the pulse. This oscillation is of little relevance, however, since the amplitude of the induced dipole which is related to the excited-state population is extremely small. It dips down to 12 725 cm^{-1} during the main peak of the pulse and oscillates with its intrinsic frequency close to the D_2 resonance superimposed with the fast beat pattern after the main peak is over. While the beat patterns are easily resolved in the calculations where a time step of 1 fs was employed (the results shown in Fig. 4 are not convoluted with a Gaussian representing the effect of the probe pulse), they require a probe pulse with FWHM of 100 fs or less and a sufficiently good signal-to-noise ratio to be observed experimentally in, e.g., the excited-state population. In the experiment discussed here the comparatively long duration of the probe pulse does not allow for the observation of this beat pattern.

The coherent transients are solely due to electronic transitions as explained in detail below in Sec. V. Their dynamics can therefore also be modeled in the framework of dressed states of a two-level system. This approach has the advantage of yielding analytic expressions which describe the coherent interactions causing the dipole modulations [32].

V. COMPARISON OF THEORETICAL AND EXPERIMENTAL RESULTS

A detailed comparison of the quantum dynamical calculations to the experimental results is presented in the following. A typical pump-probe signal recorded in an experiment with excitation frequency near the D_2 line is depicted by the black curves in Fig. 5, while the gray curves represent the excited-state population obtained in the calculations after convolution with the probe pulse (cf. Sec. II). For a chosen cut-off position below the D_2 resonance (here 10 cm^{-1}), a constant molecular ion signal is measured at negative time delays where the probe pulse precedes the pump pulse, cf. Fig. 5(a). For zero delay, the pump and probe pulses coincide in time and a peak of about 0.5 ps width is observed. For positive time delays where the pump pulse precedes the probe pulse, an increased molecular ion signal occurs with characteristic oscillations that are fully damped after a few picoseconds. An excellent agreement between the measured pump-probe data and the simulated excited-state population in the attractive potentials of the $5s+5p_{3/2}$ is observed for positive delays. The finite offset of the experimental signal at negative delays is absent in the theoretical curve. The calculations are done for a single pump pulse, while the experiments operate with a high repetition rate, 100 kHz. The signal at negative delays is therefore attributed to molecules in the electronic ground state that were produced by the previous pump pulse and spontaneous emission [20]. This effect is not taken into account in the calculations.

When the atomic resonance is included in the pump pulse spectrum [Fig. 5(b)], the total pulse energy needs to be reduced by 50% with an optical gray filter to avoid a too strong perturbation of the ultracold cloud. In this case, a higher ion
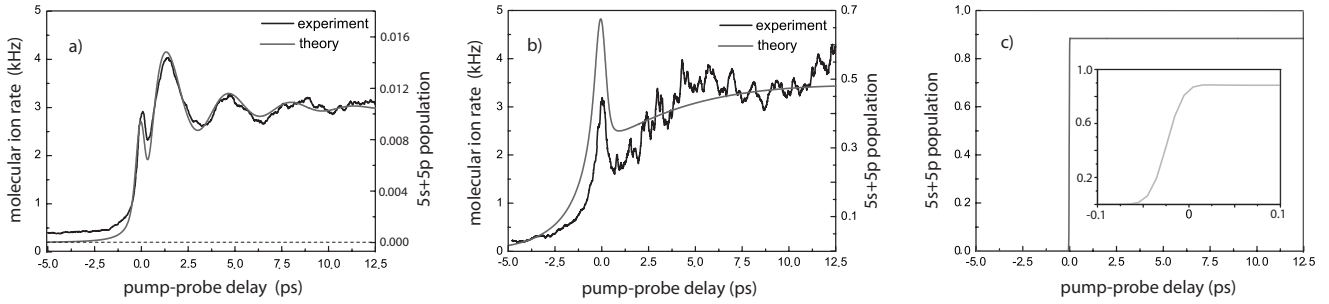
FIG. 5. Experimental (black) and theoretical (gray) pump-probe signals for pump pulses with spectral cutoff (a) 10 cm^{-1} red to the D_2 line resonance, (b) directly on the resonance frequency, and (c) theoretical signal for a pump pulse without spectral cutoff (transform-limited pulse).

signal compared to that obtained with a cut to the red of the resonance frequency is observed for positive time delays. The characteristic oscillations at positive delay disappear almost completely, cf. Fig. 5(b). When a transform-limited pulse is considered in the calculation, the population is quickly transferred to the excited-state, and no oscillations are observed in Fig. 5(c) (the inset shows a zoom of 200 fs around zero delay). In the experiment, a transform-limited pulse led to a destruction of the sample. Figure 5 illustrates that the transient oscillations depend strongly on the spectral cutoff of the pump pulse spectrum.

Figure 6 shows the time-resolved molecular ion signal for different spectral cutoffs below the D_1 and D_2 line resonances in comparison with the corresponding quantum dynamical calculations. Generally, the pump-probe spectra obtained by exciting the ultracold ensemble near the D_1 and D_2 line resonances are very similar. A notable difference is observed in the Rb$_2^+$ count rate which is larger for excitation near the D_2 line and positive delays. This is attributed to the larger dipole moment for the $5s \rightarrow 5p_{3/2}$ transition. When the sample is irradiated by the probe pulse only, a constant level of molecules is detected. This signal is due to molecules that are produced by the trapping light. It is subtracted as background from each pump-probe spectrum.

In Fig. 6 the "detuning" of the spectral cut position with respect to the atomic resonance increases from top to bottom. A decreasing mean ion signal at positive time delays is observed for increasing cutoff position for excitation close to both the D_1 and D_2 line resonance. Moreover, the characteristic oscillations at positive time delay decrease in their period and amplitude as the cutoff position is moved further away from the resonance. The decrease in oscillation period is explained in terms of the instantaneous frequency of the pump pulse. A linear dependence of the oscillation frequency on the frequency of the cutoff position was recorded, cf. Fig. 2 of Ref. [20]. This is due to the laser field oscillating with an instantaneous frequency that corresponds to the cut-off position, cf. Sec. IV. The decrease in amplitude with increasing cutoff detuning is attributed to the most important frequencies being excluded from the pulse. Moreover, the pulse energy is reduced when more frequency components are removed from the pump pulse spectrum. Then the instantaneous intensity and hence the coupling between the field and the molecular dipole become smaller.

One might expect nuclear dynamics of the excited-state wave packet to show up as oscillations in the molecular ion

signal. However, the vibrational periods of the excited-state levels that are populated, cf. Fig. 3, are at least one order of magnitude larger than the oscillation periods observed in Fig. 6. Moreover, one would expect to see wave packet revivals in the vibrational dynamics which have not been observed even when scanning the delay for very long times (up to 250 ps). In the calculations, vibrational dynamics should yield slightly different oscillation periods for the various potentials due to the different effective C_3 coefficients. However, identical oscillation periods were obtained for all potentials, independent of their character. All these observations clearly rule out molecular vibrational dynamics as origin of the observed oscillations and support their purely electronic character.

Figure 7 displays the variation in the averaged asymptotic pump-probe signals with the cut-off position. Asymptotic refers to delay times for positive delay ($t > 0$) where the oscillatory behavior is fully damped and to delay times before the signal rise for negative delay ($t < 0$, not modeled). The measured data are shown as upward triangles for positive delay and as downward triangles for negative delay. The results of the calculation were scaled to match the experimental data and are represented by a gray line (positive delay only). The insets display the ratio of the asymptotic pump-probe signals at positive and negative delay versus the cutoff position. This ratio is obtained to be about 0.3 at the D_1 line and about 0.1 at the D_2 line. As discussed in detail in Ref. [21], the nearly constant ratio indicates that the signal at negative delay, when the probe precedes the pump pulse is related to molecules that were photoassociated by a previous pump pulse and have undergone spontaneous decay to the electronic ground state. The experimental result for positive delay is well reproduced by the calculation. In particular, in accordance with the results of Fig. 6 an increase in the excited-state population is observed as the cut-off position approaches the resonance frequency.

The influence of a linear frequency chirp on the pump-probe signals is discussed with the help of Fig. 8. Measured (calculated) pump-probe spectra are shown for different positive chirps in Figs. 8(a) and 8(c) and for negative chirps in Figs. 8(b) and 8(d) for an excitation near the D_2 line resonance and a cut-off position of 8 cm^{-1} below the resonance frequency. The spectral cutoff in combination with the applied quadratic phase shift causes strong distortions of amplitude and frequency behavior during the pulse compared to the transform-limited and spectrally cut but unchirped
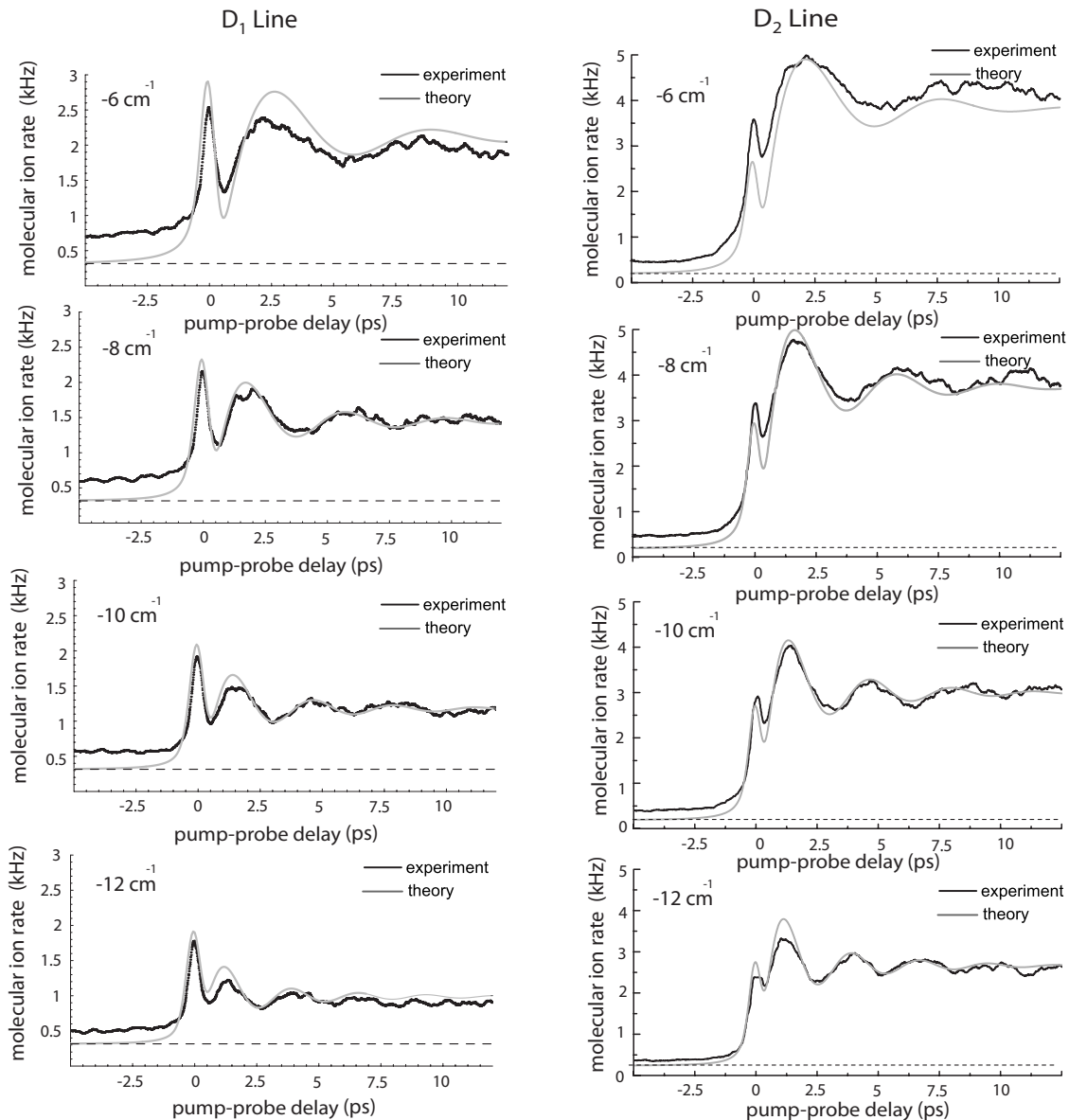
FIG. 6. Experimental (black) and theoretical (gray) pump-probe signals for pump pulses with different spectral cutoff positions red to the D_1 line resonance ($5s+5p_{1/2}$-asymptote, left) and D_2 line resonance ($5s+5p_{3/2}$-asymptote, right), respectively. The constant level of molecules measured by irradiating with the probe pulse only is indicated by the dashed lines, and the zero of the theoretical results is shifted to coincide with this level.

pulses. A frequency chirp conserves the spectral bandwidth but prolongs the pulse. Since the pulse energy remains unchanged, the peak intensities are decreased. This leads to a reduction in the detected ion signal compared to an unchirped pump pulse for both negative and positive time delays, cf. the black and gray lines in Fig. 8. Coherent transients are present also in the pump-probe spectra for chirped pump pulses. The chirp does not change their period, but it induces a shift of the zero delay peak, as indicated by the arrows in Fig. 8. This behavior is well reproduced by quantum dynamical calculations. For a positive (negative) chirp, the larger instantaneous frequencies occur after (before) the smaller ones during the pulse. The larger instantaneous frequencies are more likely to cause the off-resonant excitation of population into the excited state than the smaller ones.

This explains the shift of the zero delay peak toward later (earlier) times for positive (negative) chirps.

In previous calculations with chirped pulses, e.g., [4,5] an enhanced efficiency was proposed for chirped pulses. Here, an enhancement of the excited-state population by using linearly chirped pump pulses was not observed. This is due to the off-resonant character of the excitation, cf. Sec. III. References [4,5] describe resonant excitation, i.e., only levels with free-bound transition frequencies within the spectrum of the pulse were addressed. Moreover, picosecond pulses were considered where some vibrational dynamics occurs during the pulse. The proposed enhancement then results from an interplay between the wave packet rolling down the potential and the coupling with the field. This cannot be expected in our case. Note that such an interplay between nuclear and
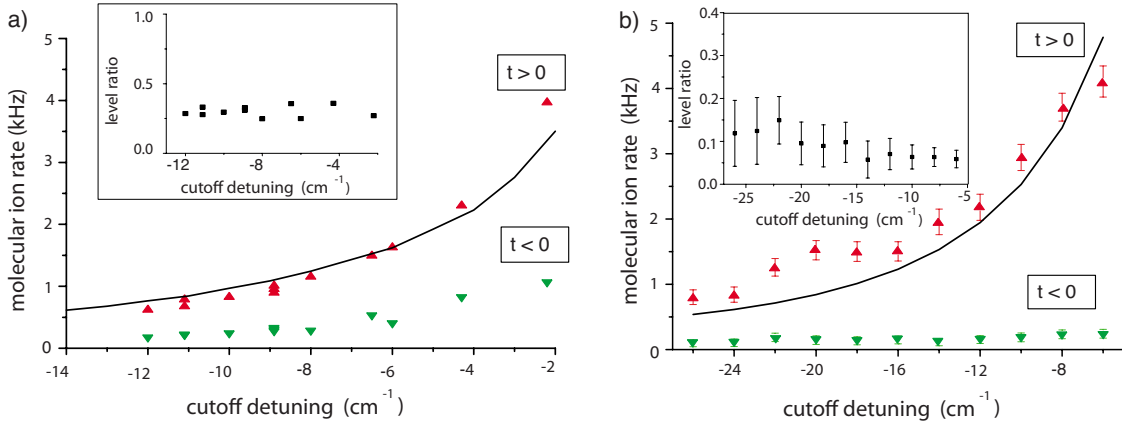
FIG. 7. (Color online) Averaged asymptotic Rb_2^+ rates at positive ($t > 0$) and negative ($t < 0$) delay versus spectral cut-off position. The experimental results are in good agreement with theory for both (a) D_1 and (b) D_2 resonance. The insets show the ratio of the asymptotic signals at positive and negative delay for a given cutoff position.

electronic dynamics has been recently observed for nanosecond pulses, demonstrating coherent control of ultracold collisions with frequency-chirped light [33]. In addition to reducing excitation efficiency, the linear chirps affect the dynamics of the induced dipole. This can be seen in the shift of the first peak relative to the oscillations indicated by the arrows in Fig. 8 for positive and negative chirps. As discussed above, the oscillations arise from the energy exchange between the induced dipole and the electric field of the pulse. They can therefore be expected to be very sensitive to phase manipulations of the pulse which also affect the relative phase between dipole and field.

Since the molecular dynamics is reduced to the electronic dynamics, i.e., to that of a two-level system, the interaction
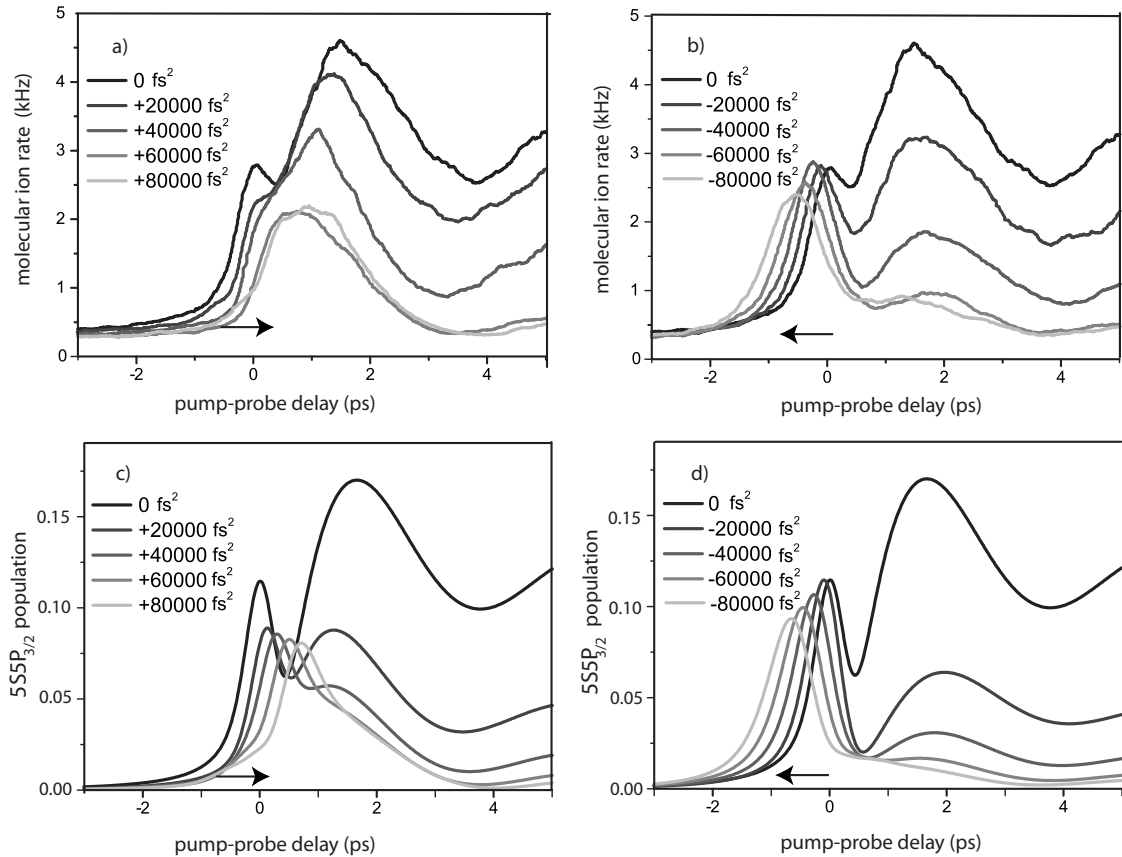

FIG. 8. Pump-probe spectra for different quadratic spectral phase shifts, i.e., linear chirps and a pump pulse cutoff position of 8 cm^{-1} below the D_2 line resonance frequency. Experimental (theoretical) results are shown in top (bottom) panels. As indicated by the arrows, [(a) and (c)] a positive chirp induces a shift of the zero delay peak to positive time delays, whereas [(b) and (d)] a negative chirp causes the opposite effect.
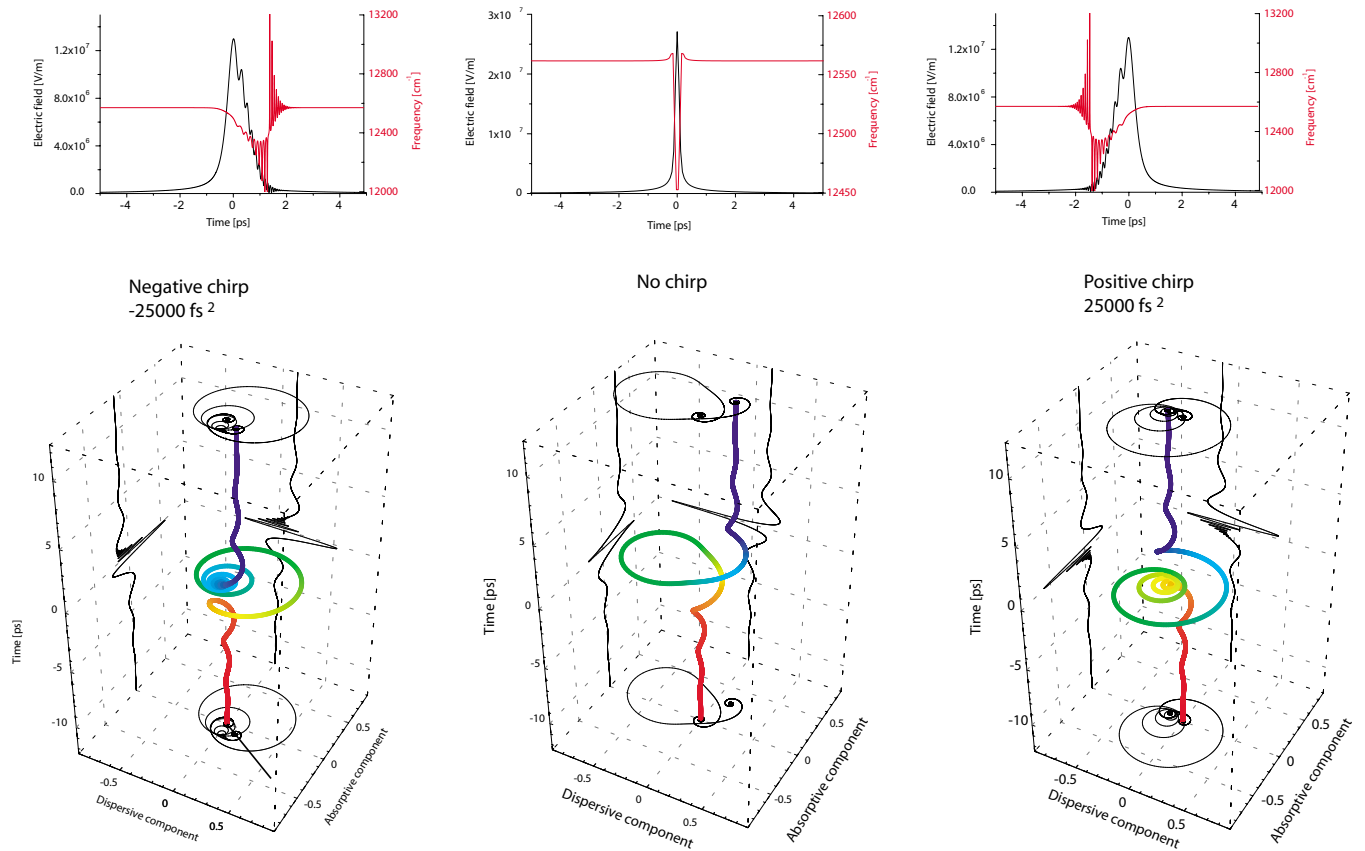
FIG. 9. (Color online) Top panel: electric field (black lines) and instantaneous frequency (red line) of pulses with negative, no, and positive chirp. Bottom panel: absorptive and dispersive components of the system Bloch vector as chirped, spectrally cut pump pulses interact with the system. Linear chirps result in different final phases of induced dipole and pulse field, causing phase shifts in the coherent transient modulations.

between the molecule and the field can also be analyzed in terms of the evolution of the Bloch vector [32]. Figure 9 shows the dispersive and absorptive components, $u(t) = \rho_{ge}(t) + \rho_{eg}(t)$ and $v(t) = i[\rho_{ge}(t) - \rho_{eg}(t)]$, of the Bloch vectors for chirped and unchirped pulses versus time [34]. For unchirped pulses, cf. middle graph in Fig. 9, the Bloch vector moves merely through a single loop in the $u-v$ plane during the main pulse peak. For chirped pulses the Bloch vectors perform rapid rotations in the $u-v$ plane during the main pulse peak as the instantaneous frequency of the pulse varies, cf. Fig. 4(a). For negative (positive) chirps, cf. the left (right) graph of Fig. 9, the rapid rotations occur before (after) $t=0$. As a result the final position of the Bloch vector in the $u-v$ plane is different for different sign of the chirp. The modulations on the absorptive component that are responsible for the energy exchange between molecule and field then oscillate with a phase offset compared to zero chirp.

VI. CONCLUSIONS

We have presented theoretical calculations describing femtosecond pump-probe photoassociation experiments [20,21]. Two colliding rubidium atoms in their electronic ground state are excited by the pump pulse into bound levels and continuum states near the $5s+5p_{1/2}$ and $5s+5p_{3/2}$ as-

ymptotes. They are ionized by a second time-delayed probe pulse and detected by a mass spectrometer. The model considers only the pump pulse explicitly while accounting for the finite width of the probe pulse by convolution with a Gaussian. The pump pulse was modeled according to the experimental conditions. In particular, spectral cuts of amplitude and quadratic spectral phases were considered. Photoassociation is observed as excitation of the two atoms into weakly bound molecular levels, mostly very close to the dissociation limit. It is attributed mainly to off-resonant excitation. The spectral cutoff produces pulses in time with very long tails giving rise to transient oscillations of the ion signal, respectively, excited-state population. Coherent transients were analyzed in terms of the field-induced dipole and the relative phase between system and field. Pump pulses obtained for different cut positions and linear chirps were employed. The oscillation period of the coherent transients is directly related to the cutoff position. A negative (positive) chirp simply shifts the zero peak delay to shorter (larger) delay times. Calculations were performed for a number of different excited-state potential-energy curves correlating to both the $5s+5p_{1/2}$ and $5s+5p_{3/2}$ dissociation limits yielding, however, identical oscillation periods of the coherent transients. This indicates a purely electronic character of the observed oscillations. The analysis of the two-level dynamics

was further confirmed by inspection of the system's Bloch vector.

The experiments modeled in this paper have provided evidence for femtosecond photoassociation. The off-resonant excitation of molecular levels and the coherent transients both clearly demonstrate that the observed phenomena are beyond the sudden approximation. However, the molecules created by the femtosecond pump pulse are extremely weakly bound—they do not provide a suitable starting point for the application of a dump pulse in order to create ultracold molecules in their electronic ground state. In future experiments, the pulses should therefore be better adapted to the time scales of the problem. In particular, a bandwidth of a few wave numbers should be best to create a spatially localized excited-state wave packet [5] that can subsequently be dumped to the electronic ground state [6,7].

Theoretical estimates predict a moderate photoassociation efficiency of about one molecule per pulse for a magneto-optical trap (MOT) [8]. The efficiency is limited by the comparatively small pair density at the distances where photoas-

sociation is effective. Future experiments on short-pulse photoassociation should therefore be combined with efforts to increase the pair density. Two routes can be pursued toward this goal. (i) The atoms can be cooled further to reach the quantum degenerate regime. Compared to the highest possible densities in a MOT, about three orders of magnitude can be gained this way. (ii) External fields can be employed to enhance the pair density at short and intermediate distances. For example, an increase in the photoassociation efficiency of up to five orders of magnitude is predicted for magnetic field control in Feshbach-optimized photoassociation [35]. Pursuing one of these routes or a combination thereof, an efficiency of 10^3 molecules per pulse or more is to be expected in photoassociation with picosecond pulses.

ACKNOWLEDGMENTS

[1] K. M. Jones, E. Tiesinga, P. D. Lett, and P. S. Julienne, Rev. Mod. Phys. **78**, 483 (2006).

[2] F. Masnou-Seeuws and P. Pillet, Adv. At., Mol., Opt. Phys. **47**, 53 (2001).

[3] A. Vardi, D. Abrashkevich, E. Frishman, and M. Shapiro, J. Chem. Phys. **107**, 6166 (1997).

[4] J. Vala, O. Dulieu, F. Masnou-Seeuws, P. Pillet, and R. Kosloff, Phys. Rev. A **63**, 013412 (2000).

[5] E. Luc-Koenig, R. Kosloff, F. Masnou-Seeuws, and M. Vatasescu, Phys. Rev. A **70**, 033414 (2004).

[6] C. P. Koch, E. Luc-Koenig, and F. Masnou-Seeuws, Phys. Rev. A **73**, 033408 (2006).

[7] C. P. Koch, R. Kosloff, and F. Masnou-Seeuws, Phys. Rev. A **73**, 043409 (2006).

[8] C. P. Koch, R. Kosloff, E. Luc-Koenig, F. Masnou-Seeuws, and A. Crubellier, J. Phys. B **39**, S1017 (2006).

[9] E. A. Shapiro, M. Shapiro, A. Pe'er, and J. Ye, Phys. Rev. A **75**, 013405 (2007).

[10] U. Poschinger, W. Salzmann, R. Wester, M. Weidemüller, C. P. Koch, and R. Kosloff, J. Phys. B **39**, S1001 (2006).

[11] J. G. Danzl, E. Haller, M. Gustavsson, M. J. Mark, R. Hart, N. Bouloufa, O. Dulieu, H. Ritsch, and H.-C. Nägerl, Science **321**, 1062 (2008).

[12] K.-K. Ni, S. Ospelkaus, M. H. G. de Miranda, A. Pe'er, B. Neyenhuis, J. J. Zirbel, S. Kotochigova, P. S. Julienne, D. S. Jin, and J. Ye, Science **322**, 231 (2008).

[13] J. Deiglmayr, A. Grochola, M. Repp, K. Mörtlbauer, C. Glück, J. Lange, O. Dulieu, R. Wester, and M. Weidemüller, Phys. Rev. Lett. **101**, 133004 (2008).

[14] F. Lang, K. Winkler, C. Strauss, R. Grimm, and J. Hecker Denschlag, Phys. Rev. Lett. **101**, 133005 (2008).

[15] C. P. Koch, J. P. Palao, R. Kosloff, and F. Masnou-Seeuws, Phys. Rev. A **70**, 013402 (2004).

[16] A. Pe'er, E. A. Shapiro, M. C. Stowe, M. Shapiro, and J. Ye, Phys. Rev. Lett. **98**, 113004 (2007).

[17] W. Salzmann *et al.*, Phys. Rev. A **73**, 023414 (2006).

[18] N. Dudovich, D. Oron, and Y. Silberberg, Phys. Rev. Lett. **88**, 123004 (2002).

[19] A. Monmayrant, B. Chatel, and B. Girard, Phys. Rev. Lett. **96**, 103002 (2006).

[20] W. Salzmann *et al.*, Phys. Rev. Lett. **100**, 233003 (2008).

[21] T. Mullins *et al.*, Phys. Rev. A **80**, 063416 (2009).

[22] At this time the electric field is reduced by seven orders of magnitude compared to the peak.

[23] S. J. Park, S. W. Suh, Y. S. Lee, and G.-H. Jeung, J. Mol. Spectrosc. **207**, 129 (2001).

[24] A. Marte, T. Volz, J. Schuster, S. Dürr, G. Rempe, E. G. M. van Kempen, and B. J. Verhaar, Phys. Rev. Lett. **89**, 283202 (2002).

[25] R. F. Gutterres, C. Amiot, A. Fioretti, C. Gabbanini, M. Mazzoni, and O. Dulieu, Phys. Rev. A **66**, 024502 (2002).

[26] H. Wang, P. L. Gould, and W. C. Stwalley, J. Chem. Phys. **106**, 7899 (1997).

[27] V. Kokoouline, O. Dulieu, R. Kosloff, and F. Masnou-Seeuws, J. Chem. Phys. **110**, 9865 (1999).

[28] K. Willner, O. Dulieu, and F. Masnou-Seeuws, J. Chem. Phys. **120**, 548 (2004).

[29] R. Kosloff, J. Phys. Chem. **92**, 2087 (1988).

[30] All full widths at half maximum are taken with respect to the intensity profile.

[31] M. Shapiro and P. Brumer, *Principles of the Quantum Control of Molecular Processes* (Wiley Interscience, New York, 2003).

[32] M. Albert, T. Mullins, S. Götz, W. Salzmann, R. Wester, and M. Weidemüller, J. Mod. Opt. **55**, 3359 (2008).

[33] M. J. Wright, J. A. Pechkis, J. L. Carini, S. Kallush, R. Kosloff, and P. L. Gould, Phys. Rev. A **75**, 051401(R) (2007).

[34] The inversion component, $\sigma_z(t)$, plotted vertically in the Bloch sphere is small throughout the interaction.

[35] P. Pellegrini, M. Gacesa, and R. Côté, Phys. Rev. Lett. **101**, 053201 (2008).